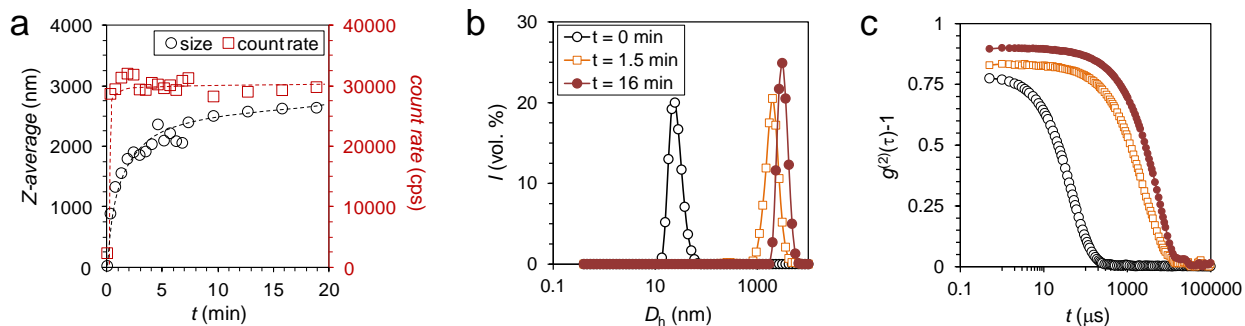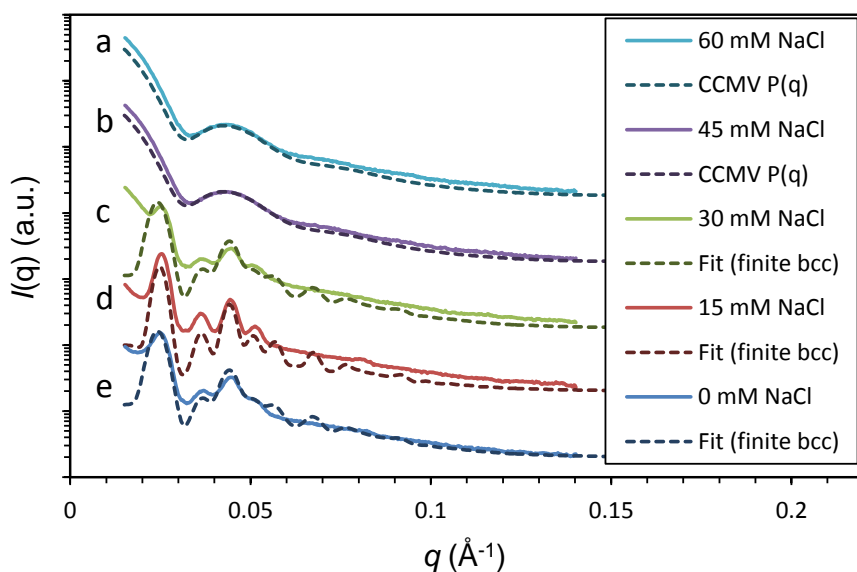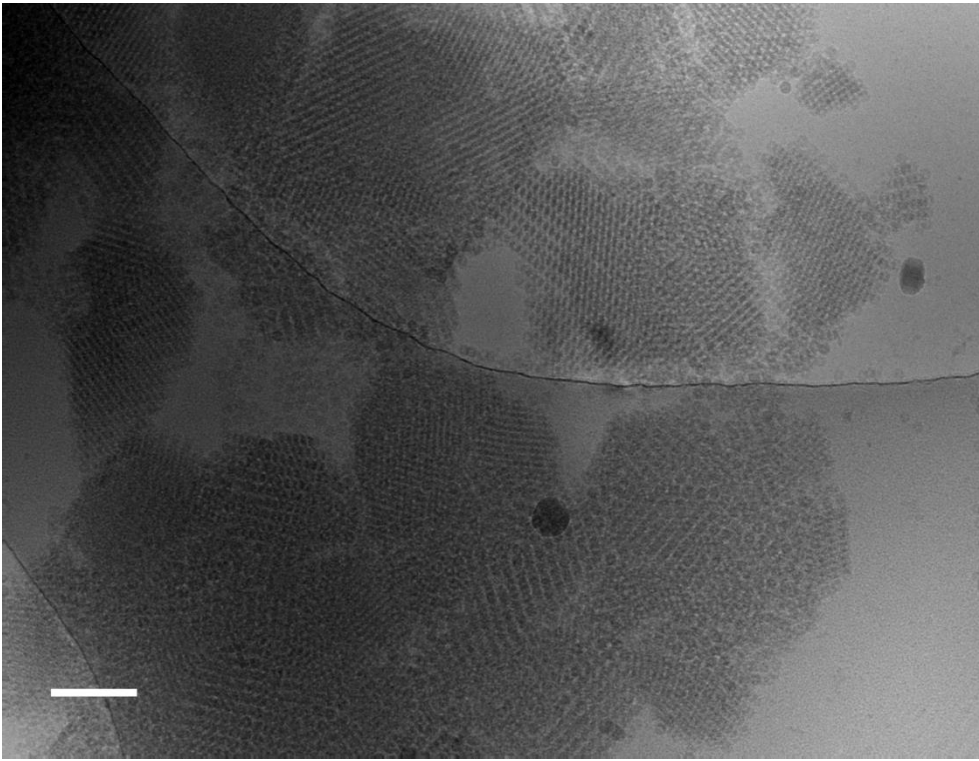1. **Supplementary Figures:**

Supplementary Figure 1. Timescales for the assembly of CCMV-avidin complexes measured by DLS.
a, Changes in the Z-average and count rate monitored as a function of time after combining CCMV and avidin. **b**, Volume-averaged size-distributions observed at different time points and **c**, the corresponding second-order autocorrelation curves. The assembly process is extremely rapid and the formation of initial crystallites with a diameter of hundreds of nanometres takes place in seconds. Larger assemblies are achieved within the time frame of minutes.

Supplementary Figure 2. SAXS profiles of CCMV-avidin samples at different ionic strengths (NaCl) and calculated models for the scattering. a & b, Integrated SAXS intensity from samples with the ionic strength of 60 mM and 45 mM and the calculated model for the form factor of CCMV show the presence of free CCMV particles. **c & e**, Integrated SAXS intensity from samples with the ionic strength of 30 mM and 0 mM show the formation of crystalline assemblies with small crystal domain sizes. **d**, Integrated SAXS intensity from a 15 mM sample yields the best resolved Bragg reflections. The calculated models for the scattering are based on bcc crystals formed from CCMV particles with unit cell size of 34.8 nm. SAXS profiles show the effect of ionic strength on the self-assembly of CCMV and avidin to higher-order hierarchical structures. Samples prepared in the absence of added electrolyte show heavily broadened diffraction peaks due to the low degree of order, which is a result of the high electrostatic attraction between CCMV and avidin that further leads to fast, kinetically trapped aggregation where CCMV and avidin are electrostatically locked in their positions once the aggregate is formed. The best resolved and sharpest Bragg reflections were acquired at a low ionic strength (15 mM NaCl solution), as the opposite charges are then partially screened by the ions in the solution. From this sample *hkl* reflections 110, 200, 211, 220, 310 and 420 were identified and the measured reflections were in good agreement with a bcc structure with a unit cell size of 34.8-35.0 nm. At high ionic strengths (45 mM or higher NaCl concentration) the electrostatic self-assembly of CCMV and avidin does not take place, which can be seen in that the scattering form factor of CCMV dominates the SAXS profile. Apart from the theoretical scattering curves in Fig. 3 (which were calculated with PowderCell[1]), all other curves were calculated with Scatter[2,3] software.

Supplementary Figure 3. Low-magnification TEM image of CCMV-Avidin crystals. Image shows multiple randomly oriented crystal domains with a bcc lattice. The crystal domain sizes range from roughly 100 nm to roughly 1 μm. The CCMV is easily distinguished from the micrographs and the cryo-TEM experiments are in excellent agreements with the SAXS results. Scale bar is 200 nm.
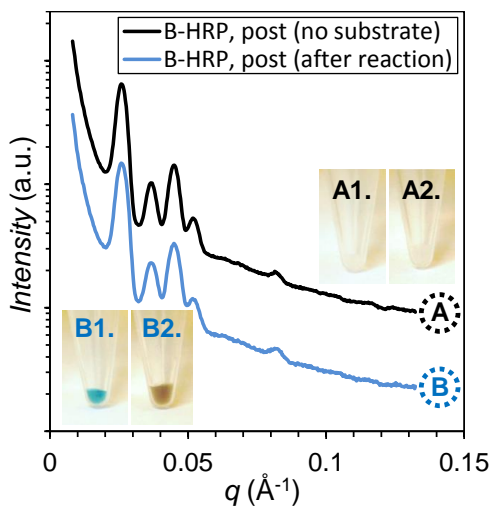
Supplementary Figure 4. SAXS scattering curves of CCMV-avidin-HRP crystals. SAXS curves measured from samples before (A) and after (B) the addition of 10 μl of TMB substrate solution (1 ml of tetramethylbenzidine (TMB) 1 mg ml^{-1} in DMSO), 9 ml of NaAc buffer (pH 5, 15 mM NaAc) and 2 μl of hydrogen peroxide) were almost identical. Insets: photographs of SAXS samples prior to measurement. Sample B1 shows visually the evolution of a blue colour at an intermediate stage, which gradually turns brown as the reaction completes (Sample B2). SAXS curves were measured from samples A2 and B2.
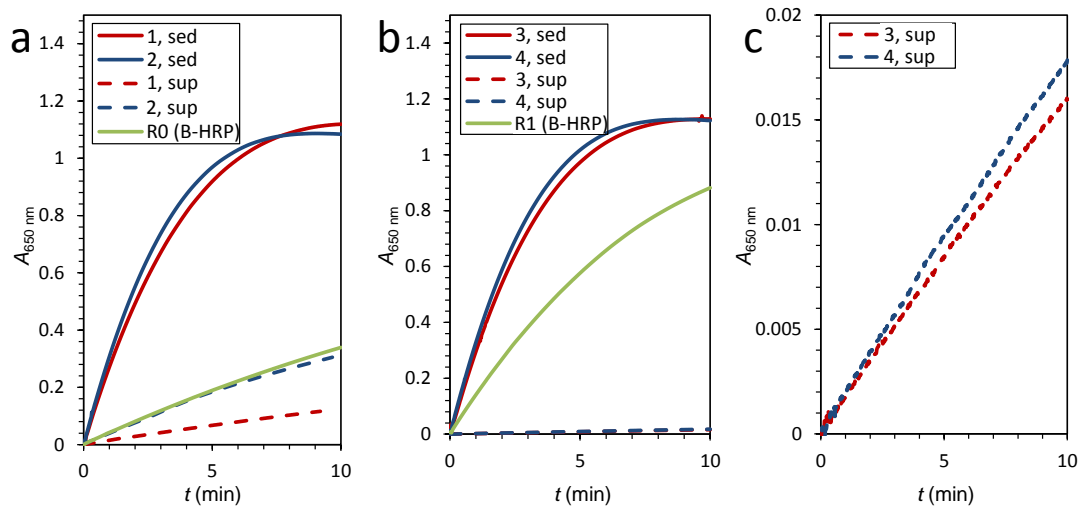
Supplementary Figure 5. Progress curves for TMB – B-HRP enzyme reaction. a, **B-HRP** functionalized crystals separated by centrifugation. **b**, Four times washed **B-HRP** functionalized, **c**, Magnification of the lowest part of graph b showing the low catalytic activity of the supernatant in the four times washed samples. Sample components are listed in the Supplementary Table 2 and catalytic activities in Supplementary Table 3.
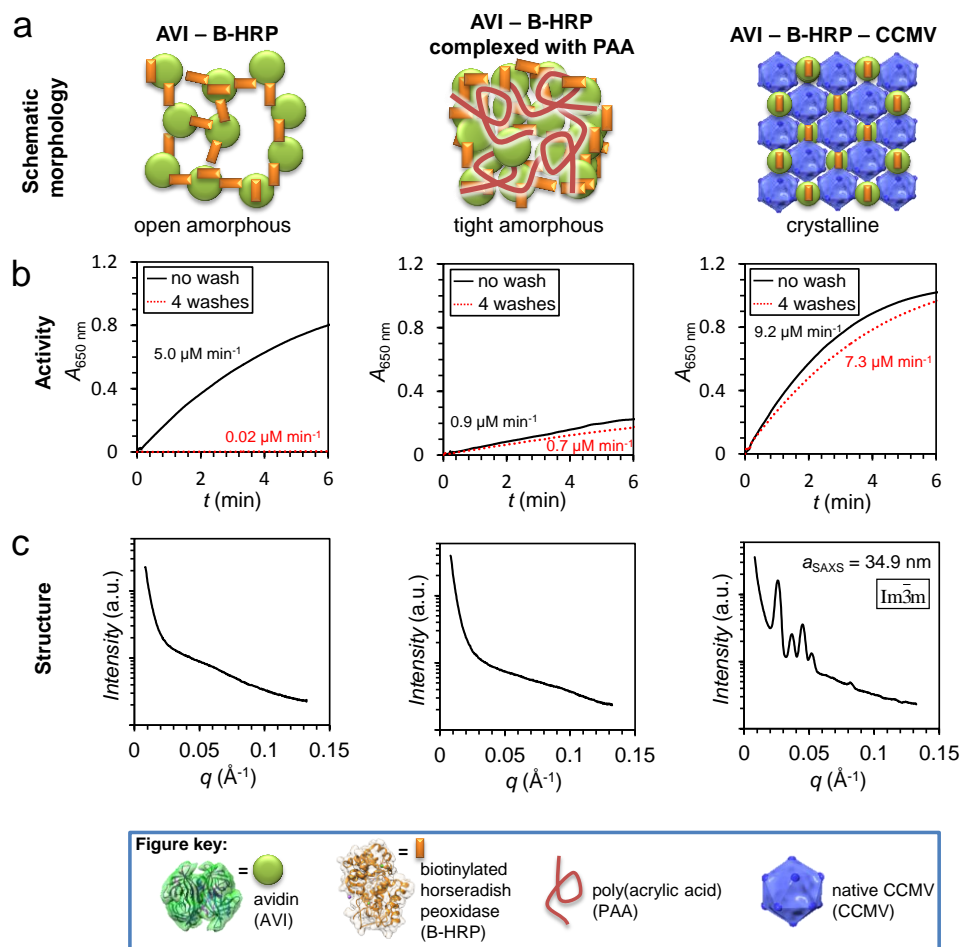
Supplementary Figure 6. Effect of complex morphology on enzyme activity. a, Schematic presentation of the complexes. **b**, Progress curves before and after washing as well as the derived initial velocities. Only crystalline AVI–B-HRP–CCMV sample show high activity before and after washing. **c**, SAXS curves measured from the complexes. Samples without CCMV do not exhibit a crystal structure. Sample components are listed in the Supplementary Table 4.
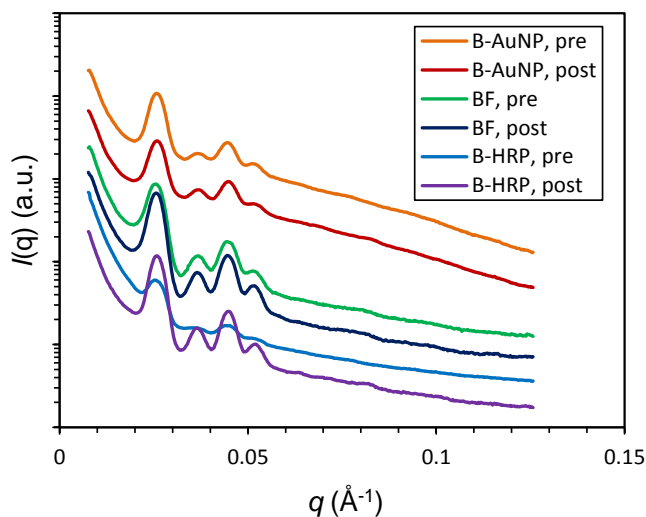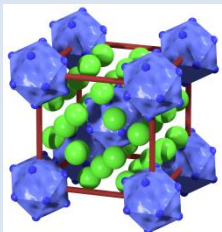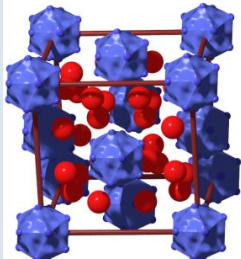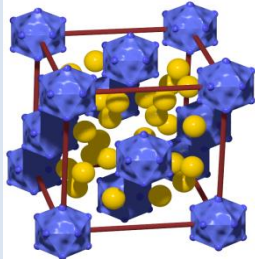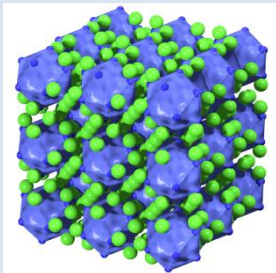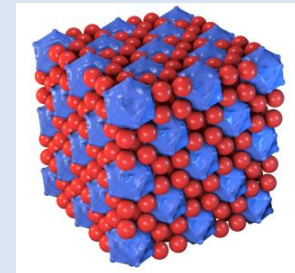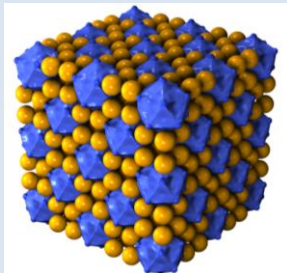
Supplementary Figure 7. SAXS profiles of differently functionalized CCMV-avidin samples at 15 mM ionic strengths (NaCl). Integrated SAXS profiles from samples pre-or post-functionalized with 5 nm **B-AuNP**, **BF** and **B-HRP**. All scattering profiles show diffraction peaks corresponding to the same bcc structure as in the non-functionalized CCMV-avidin crystal, which shows that the functionalization does not affect the crystal structure. In the SAXS profile of the pre-functionalized **B-HRP** sample the diffraction peaks are not as well resolved as in the other SAXS profiles, which shows that pre-functionalization using **B-HRP** restrains proper crystallization of the functionalized CCMV-avidin crystals.
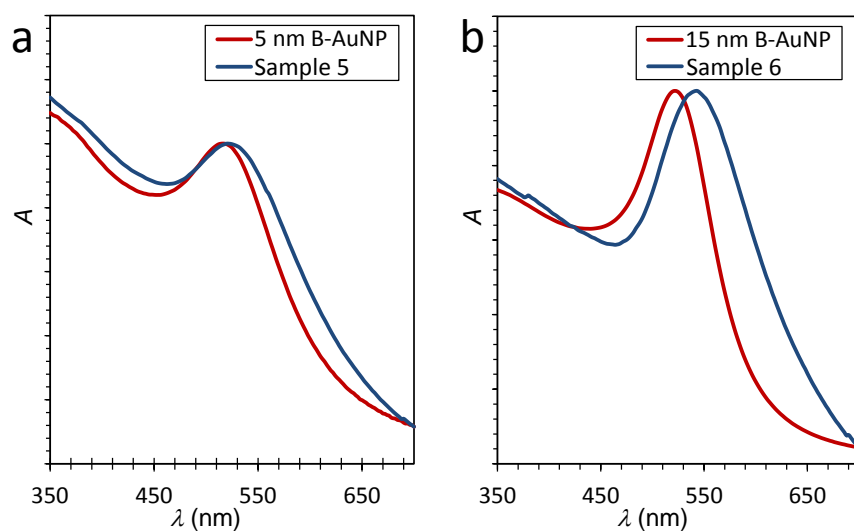
Supplementary Figure 8. **UV-Vis spectra for pure B-AuNP solutions and B-AuNP functionalized CCMV-avidin crystals. a**, The absorption maximum for free 5 nm **B-AuNPs** is at 516 nm. The absorption maximum for 5 nm **B-AuNP** post-functionalized CCMV-avidin crystal (Sample 5) is shifted to 520 nm. **b**, The absorption maximum for free 15 nm **B-AuNPs** is at 522 nm. The absorption maximum for 15 nm **B-AuNP** post-functionalized CCMV-avidin crystal (Sample 6) is shifted to 542 nm. A constant baseline is subtracted from Sample 5 and Sample 6 data to take into account the scattering from CCMV-avidin assemblies. See also the supplementary Note 3.

2. **Supplementary Tables:**

Supplementary Table 1. Unit cell details for the suggested binary structures.

|	$(\text{CCMV-avidin}_{12})^{bcc}$	$(\text{CCMV-PAMAM-G6}_{8})^{fcc}$	$(\text{CCMV-AuNP}_{8})^{fcc}$ (see note[1])
Bravais lattice	*body-centred cubic*	*face-centred cubic*	*face-centred cubic*
Space group (number)	$I m\bar{3}m$ (229)	$F m\bar{3}m$ (225)	$F m\bar{3}m$ (225)
Unit cell size (lattice parameter a)	35.0 nm	40.5 nm	40.4 nm
Protein cage centre-to-centre distance	30.3 nm	28.6 nm	28.6 nm
Particles in unit cell	26 (2 CCMV, 24 avidin)	36 (4 CCMV, 32 PAMAM)	36 (4 CCMV, 32 AuNP)
Primitive vectors	$A_1 = -\frac{1}{2}\,a\mathbf{X} + \frac{1}{2}\,a\mathbf{Y} + \frac{1}{2}\,a\mathbf{Z}$ $A_2 = \frac{1}{2}\,a\mathbf{X} - \frac{1}{2}\,a\mathbf{Y} + \frac{1}{2}\,a\mathbf{Z}$ $A_3 = \frac{1}{2}\,a\mathbf{X} + \frac{1}{2}\,a\mathbf{Y} - \frac{1}{2}\,a\mathbf{Z}$	$A_1 = \frac{1}{2}\,a\mathbf{Y} + \frac{1}{2}\,a\mathbf{Z}$ $A_2 = \frac{1}{2}\,a\mathbf{X} + \frac{1}{2}\,a\mathbf{Z}$ $A_3 = \frac{1}{2}\,a\mathbf{X} + \frac{1}{2}\,a\mathbf{Y}$	$A_1 = \frac{1}{2}\,a\mathbf{Y} + \frac{1}{2}\,a\mathbf{Z}$ $A_2 = \frac{1}{2}\,a\mathbf{X} + \frac{1}{2}\,a\mathbf{Z}$ $A_3 = \frac{1}{2}\,a\mathbf{X} + \frac{1}{2}\,a\mathbf{Y}$
Basis vectors x,y,z (CCMV) (cationic species)	$B_1 = (0\mathbf{X}, 0\mathbf{Y}, 0\mathbf{Z})$ $B_2 = (0\mathbf{X}, 0.33\mathbf{Y}, 0.33\mathbf{Z})$	$B_1 = (0\mathbf{X}, 0\mathbf{Y}, 0\mathbf{Z})$ $B_2 = (0.35\mathbf{X}, 0.35\mathbf{Y}, 0.35\mathbf{Z})$	$B_1 = (0\mathbf{X}, 0\mathbf{Y}, 0\mathbf{Z})$ $B_2 = (0.35\mathbf{X}, 0.35\mathbf{Y}, 0.35\mathbf{Z})$
Unit cell image **CCMV: blue particles** **Avidin: green spheres** **PAMAM: red spheres** **AuNP: yellow spheres** **(CCMV diameter has been reduced for clarity)**	 (see note[2])	 (see note[3])	 (see note[3])
Particle packing visualized, colour code as above			

[1] This data has been reported by us previously in the Supplementary Reference 4 and is shown here for comparison

[2] Illustration of the suggested $(\text{CCMV-avidin}_{12})^{bcc}$ structure. **a**, Unit cell showing only the 12 avidins, which are not shared between adjacent unit cells. **b**, Unit cell showing only the 36 avidins. **c**, Unit cell with 5 CCMV particles (top four particles omitted) and avidins. **d**, Unit cell with all CCMV particles and avidins.

a **b** **c** **d**
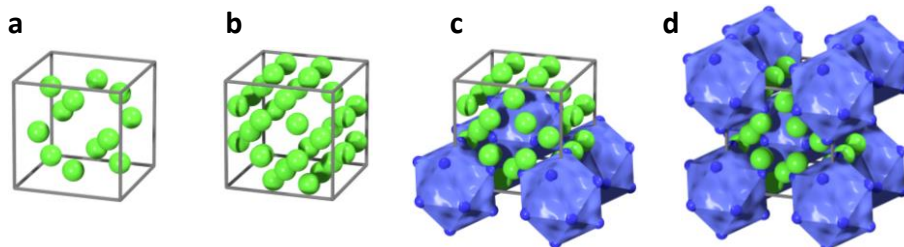
[3] Comparison to the previously reported $(\text{CCMV-AuNP}_{8})^{fcc}$ structure (and the suggested $\text{CCMV-PAMAM-G6}_{8})^{fcc}$ structure, which has a similar particle arrangement). **a**, Unit cell showing only the simple cubic arrangement of eight AuNPs located at the octahedral void in the centre of the unit cell. **b**, Unit cell showing only the 32 AuNPs. **c**, Unit cell with 9 CCMV particles (top five particles omitted) and AuNPs. **d**, Unit cell with all CCMV particles and AuNPs.

a **b** **c** **d**
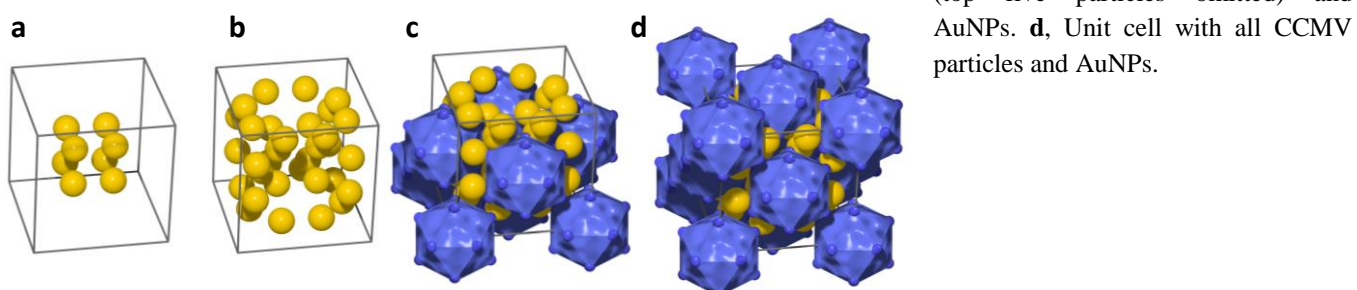
Supplementary Table 2. List of the amounts of the different components in the **B-HRP** functionalized samples (1-4) and **B-HRP** reference samples (R0-R2).

Sample	CCMV, 10 mg ml^{-1} [µl]	avidin, 10 mg ml^{-1} [µl]	HRP stock [µl]	functionalization (pre/post)	total volume [µl]
1	2.0	1.5	1.0	pre	90
2	2.0	1.5	1.0	post	90
3	2.5	1.85	1.25	pre	30
4	2.5	1.85	1.25	post	30
R0	0	0	1.0	-	90
R1	0	0	1.25	-	30
R2	1.0	0.75	-	-	10

Supplementary Table 3. The (specific) catalytic activities of sediment and supernatant of functionalized crystal samples. For samples 1 and 2 (non-washed) the sediment containing large visible crystallite aggregates had a 8.5 to 19.7 times higher specific catalytic activity than the clear supernatant. For samples 3 and 4 (four times washed) the specific catalytic activity of the sediment was 186 to 189 times higher than the catalytic activity of the supernatant.

Sample	1, sed.	2, sed.	1, sup.	2, sup.	3, sed.	4, sed.	3, sup.	4, sup.	HRP, ref.
V_0 [µM min^{-1}]	7.1	8.2	0.36	0.96	7.8	8.7	0.042	0.046	3.5
specific A_{cat} [µM µl^{-1} min^{-1}]	1.8	2.1	0.091	0.24	2.0	2.2	0.010	0.012	0.87

Supplementary Table 4. Sample components for AVI-B-HRP complexes with different structure morphology.

Sample	CCMV 10 mg ml^{-1} [µl]	Avidin 10 mg ml^{-1} [µl]	PAA 10 mg ml^{-1} [µl]	HRP stock [µl]	total volume [µl]
AVI–B-HRP	0	1.9	0	1.25	90
AVI–B-HRP–PAA	0	1.9	2	1.25	90
AVI–B-HRP–CCMV	2.5	1.9	0	1.25	90

3. Supplementary Notes:

Supplementary Note 1. Enzymatic activity – ultraviolet – visible spectrophotometry (UV-Vis) measurement of progress curves. The presence of enzymatic activity in the pre- and post-functionalized CCMV-avidin-HRP complexes was qualitatively assessed to demonstrate the HRP attachment to CCMV-avidin crystals. Four functionalized CCMV-avidin-HRP samples were prepared, two pre-functionalized and two post-functionalized (Supplementary Table 2, samples 1-4). The calculated $n_{(HRP)} : n_{(CCMV)} : n_{(avidin)}$ component ratio of all the four samples was 1 : 10 : 400. In addition three control samples (Supplementary Table 2, samples R0-R2) were prepared. The samples were prepared in a 15 mM NaCl aqueous solution.

Sample components presented in Supplementary Table 2 were first mixed together. After two minutes of centrifugation using a table-top centrifuge (max. 6000 rpm / 2000 RCF) samples 1 and 2 were divided into 80 µl of supernatant and 10 µl of sediment. Samples 3 and 4 were washed four times by centrifuging the samples for two minutes (max. 6000 rpm / 2000 RCF) and replacing 20 µl of the supernatant by 20 µl of pure 15 mM NaCl water solution followed by a gentle mixing of the sample. After the fourth wash the sample was centrifuged for the last time and divided to 25 µl of supernatant and 5 µl of sediment.

A substrate-peroxide stock was prepared by mixing 1 ml of tetramethylbenzidine (TMB) (0.2 mg ml^{-1} in DMSO), 9 ml of NaAc buffer (pH 5, 5 mM NaAc) and 2 µl of hydrogen peroxide. When measuring the progress curves of a sample, 4 µl of either the sediment or supernatant was added to 3 ml of substrate-peroxide stock, starting the catalysis of TMB. This means that the final progress curves show the relative concentrations of active **B-HRP** in the sample sediments, supernatants and reference samples respectively. The reference samples include the same concentration of **B-HRP** as the other samples before washing or centrifugation. No centrifugation or washing was done to the reference samples.

HRP catalyses the oxidation of tetramethylbenzidine to tetramethylbenzidine diimine in the presence of hydrogen peroxide. The complete oxidation proceeds via an intermediate charge transfer complex with an absorption maximum at 652 nm and extinction coefficient $\epsilon_{652}^{complex} = 3.9 \cdot 10^4$ M^{-1} cm^{-1} (Supplementary Reference 5) which was used for determining the specific catalytic activity A_{cat} (Supplementary Table 3) of the samples. The progress curves are shown in Supplementary Fig. 5. The results show clearly that **B-HRP** is attached and concentrated in the CCMV-avidin crystals which can be separated from the solution by centrifugation. The R2

reference which did not contain any **B-HRP** did not show any catalytic activity. The reason why free **B-HRP** sample has a lower activity than the crystals is therefore related to fact that crystals can be concentrated by mild centrifugation. Activity per enzyme is still higher with free **B-HRP**.

By inspecting A_{cat} and the volumes of the sediments and the supernatants of the samples after a single centrifugation, the catalytic activity of the sediment (which composes only 10 % of the total volume) was estimated to be roughly 50-70 % of the total initial activity of the sample. The expected moderate loss of catalytic activity is attributed to unbound **B-HRP** and small protein assemblies which are not sedimenting and therefore remaining in the supernatant. Still, the active **B-HRP** is highly concentrated in the sediment and strongly bound to the CCMV-avidin crystals. Even after four washes the catalytic activity of the sediment is roughly 40 % of the total initial activity of the sample, whereas the supernatant does not have almost any catalytic activity, showing that the catalytic activity of the functionalized crystallites does not decay significantly even after multiple washes.

Supplementary Note 2. Effect of complex morphology on enzyme activity. In order to demonstrate the benefits of organising enzymes into large well-defined complexes, we compared the structure morphology of avidin functionalized with **B-HRP** (AVI–B-HRP), **B-HRP** functionalized avidin complexed with M_w 250 000 poly(acrylic acid) (AVI–B-HRP–PAA) and **B-HRP** functionalized avidin complexed with CCMV (AVI–B-HRP–CCMV) by SAXS and investigated their total enzyme activity (Supplementary Fig. 6). Here, the AVI–B-HRP adopts an open amorphous structure, which is fully water soluble. SAXS does not show distinct diffraction peaks. The initial enzyme activity of the solution is high (5.0 µM min^{-1}), but as the loose complexes cannot be separated with centrifugation, the enzyme activity dramatically reduced to 0.02 µM min^{-1} after four washing steps. Also the AVI–B-HRP–PAA is devoid a crystal structure, but here tight amorphous complexes are formed, which can be readily separated. The enzyme activity in sample is relatively low (0.9 µM min^{-1}) due to the amorphous aggregation, but the activity is not significantly affected by the washing steps. In the AVI–B-HRP–CCMV sample the expected bcc crystal structure with $a = 34.9$ nm is observed. The enzyme activity of crystalline assemblies is high (9.2 µM min^{-1}) and the sample can clearly by concentrated and washed multiple times with only limited loss of the enzyme.

The AVI-B-HRP samples included only avidin functionalized by HRP (1 HRP unit per 10 avidin units). The AVI-B-HRP-PAA samples were prepared by functionalizing avidin with HRP and adding it to a PAA solution, which resulted in instant precipitation of the AVI-B-HRP-PAA

aggregates. The AVI-B-HRP-CCMV samples were prepared by first mixing CCMV and avidin resulting in rapid precipitation of the CCMV-avidin self-assemblies, which were further functionalized with **B-HRP** (Supplementary Table 4). The non-washed samples were centrifuged (2 minutes at max. 2000 RCF) and divided to 80 µl of supernatant and 10 µl of sediment. All samples were prepared in 15 mM NaCl solution. Washed samples were prepared similarly but the samples were washed four times before final centrifugation (2 min., 2000 RCF) and division to 80 µl of supernatant and 10 µl of sediment. Here one washing cycle includes centrifugation (2 min., 2000 RCF) and replacing 70 µl of the supernatant by 70 µl of water. When measuring the progress curves of the samples the sediment was added to 3 ml of substrate-peroxide stock.

Supplementary Note 3. Absorption spectra measurements – Shift in the surface plasmon resonance wavelength. Two separate CCMV-avidin samples were prepared (15 mM NaCl). Biotinylated AuNPs (Sample 5: 5 nm **B-AuNP**, 3.47 mg ml^{-1}; Sample 6: 15 nm **B-AuNP**, 2.81 mg ml^{-1}) were sequentially added to the samples until the crystals were saturated. The samples were gently mixed and centrifuged between each AuNP addition. After functionalization the sediment was washed and centrifuged repeatedly to remove any unbound AuNPs. The absorption spectra presented in Supplementary Fig. 8 show that the plasmonic resonance is clearly red shifted in the AuNP functionalized CCMV-avidin crystals in comparison to pure AuNP solutions. When the crystals are functionalized using 5 nm **B-AuNPs** the plasmon resonance is shifted moderately from 516 nm to 520 nm. The plasmon resonance shift for the 15 nm **B-AuNPs** is more pronounced, as expected, and the plasmon resonance is shifted from 522 nm to 542 nm. The shifting of the plasmon resonance is attributed to the dense coating of AuNPs on the surface of the CCMV-avidin crystals which leads to plasmon coupling between the AuNPs.

Supplementary Note 4. Preparation of materials. Detailed CCMV preparation is described elsewhere.[6] According to manufacturer, the amount of biotin on the gold surface was 0.04 units per nm^2, which equals to approximately three biotin units per 5 nm gold core and 28 biotin units per 15 nm gold core.

4. Supplementary Discussion:

Supplementary Discussion 1. Suggested binary structures. The bcc structure of CCMV-avidin crystals and the fcc structure of CCMV-PAMAM-G6 crystals both include tetrahedral and octahedral voids as CCMV particles are located in the lattice points of the unit cells. Assuming a spherical 28 nm diameter CCMV particle, a close packed bcc structure would have a unit cell size of 32.3 nm as a close packed fcc structure would have a unit cell size of 39.6 nm. According to SAXS data the unit cell size of the final bcc structure of CCMV-avidin complex is 35.0 nm as the unit cell size of the fcc structure of CCMV-PAMAM-G6 is 40.5 nm.

The diffraction peak positions in the SAXS profile measured from the CCMV-PAMAM-G6 reference sample matched well with the theoretical hkl reflections of a fcc structure with a unit cell size of 40.5 nm. hkl reflections 111, 220, 311, 422, 600 (442), 620 and 731 (553) could be identified unambiguously from the SAXS profile, whereas the 200, 311, 420, 551 (711) and 640 were identified but not resolved properly due to the broadening of the diffraction peaks. The theoretical models which gave scattering profiles similar to the measured profiles included the abovementioned form factor of a hollow sphere and bcc or fcc structure for CCMV-avidin and CCMV-PAMAM-G6 crystals respectively (Supplementary Method 1).

In the CCMV-avidin unit cell the smallest centre-to-centre distance between CCMV particles is 30.3 nm leaving a 2.3 nm spacing between adjacent CCMV particles (for example between CCMV particles in positions (0,0,0) and (0.5,0.5,0.5) in the unit cell). Further, the tetrahedral voids in the CCMV-avidin unit cell have a diameter of 11.1 nm and the octahedral voids have a diameter of 7.0 nm, showing that both the tetrahedral and the octahedral voids can be occupied by avidin. In the CCMV-PAMAM-G6 fcc structure with unit cell size of 40.5 nm the centre-to-centre distance of CCMV particles is 28.6 nm and the structure is almost close packed. The diameter of the octahedral voids is in this structure 12.5 nm and the diameter of the tetrahedral voids is 7.0 nm.

In the bcc structure of CCMV-avidin crystals avidin is mainly located in the tetrahedral and octahedral voids, since the volume between two adjacent CCMV particles can be too narrow to host even one avidin. However, the CCMV particles in the CCMV-avidin crystal do not compose a close packed bcc structure and the tetrahedral and octahedral voids are overlapping, which means that avidin can still form a continuous mesh around the CCMV particles. We therefore propose that the favoured structure would be an AB_{12} where a mesh of 36 avidin particles binds one CCMV particle to the four closest CCMV neighbours. In this structure each avidin binds to three CCMV particles

so that it is closely bound to one CCMV (centre-to-centre distance 16.5 nm according to crystal coordinates) and more loosely bound to three other CCMV particles (centre-to-centre distances 19.3 nm according to crystal coordinates). It is suggested that due to avidin-avidin electrostatic repulsion and geometrical constraints not all the negative patches on CCMV are occupied by avidin in this structure and the distance between adjacent avidin particles is well maximized as avidin is distributed evenly around the CCMV particles. Each avidin has four other avidins at the same centre-to-centre distance of 10.1 nm.

5. Supplementary Methods:

Supplementary Method 1. Data analysis for small angle X-ray scattering (SAXS). A qualitative analysis of the SAXS data was carried out using Scatter software[2,3] to model the scattering profiles. In model calculations we used the scattering form factor of a hollow sphere with shell thickness d, radius R and the inner radius ($R_{in} = R - d/2$) of 8.2 ± 1.2 nm and the outer radius ($R_{out} = R + d/2$) of 12.2 ± 1.8 nm. Values correspond well to the literature values which are: 10.4 nm for the average inner radius, 9.5 nm for the minimum inner radius, 12.0 nm for the minimum outer radius and 14.2 nm for the maximum outer radius.[7] A standard deviation of 15 % is applied to the model to compensate for the non-spherical shape of the CCMV particle.

For a hollow sphere with a homogeneous shell the scattering amplitude can be calculated as:

$$F(q, R, d) = \frac{\int_{R-d/2}^{R+d/2} \frac{\sin(qr)}{qr} dr}{\int_{R-d/2}^{R+d/2} 4\pi r^2 \, dr}, \tag{1}$$

which can be further evaluated as:

$$F(q, R, d) = \frac{1}{\left(1 + \frac{d^2}{12R^2}\right)} \left[\frac{\cos \chi_R}{\chi_R^2} \frac{\sin \chi_d}{\chi_d} - \frac{\cos \chi_R}{\chi_R^2} \cos \chi_d + \frac{\sin \chi_R}{\chi_R} \frac{\sin \chi_d}{\chi_d} \right], \tag{2}$$

where $\chi_R = qR$ and $\chi_d = qd/2$. The measured scattered intensity is modelled as scattering from particles with Schulz-Zimm size distribution. When taking into account the size distributions the scattering amplitude can be averaged as:

$$F(q, R, d) = \frac{1}{\left(1 + \frac{d^2}{12R^2}\right)} \left[\langle \frac{\cos \chi_R}{\chi_R^2} \rangle_R \langle \frac{\sin \chi_d}{\chi_d} \rangle_d - \langle \frac{\cos \chi_R}{\chi_R^2} \rangle_R \langle \cos \chi_d \rangle_d + \langle \frac{\sin \chi_R}{\chi_R} \rangle_R \langle \frac{\sin \chi_d}{\chi_d} \rangle_d \right], \tag{3}$$

where the angle brackets denote the function average with respect to the distribution and the subscripts R and d denote the variable, with respect to which the average over the size distribution has been taken. The form factor $P(q)$ is calculated as:

$$\langle P(q) \rangle = \langle F^2(q) \rangle \qquad (4)$$

For ordered three-dimensional CCMV-avidin self-assemblies the scattering intensity is

$$I(q) = C_{sld}P(q)S(q) , \qquad (5)$$

where C_{sld} is a constant depending on the scattering length density and the number density of the particles and $S(q)$ is the structure factor of the unit cell.

This model was found to fit well to the CCMV-avidin sample with the highest ionic strength and no aggregation of the free particles and therefore used as the form factor when modelling the SAXS data. For calculations of the scattering profiles from aggregated CCMV-avidin samples (low ionic strength) we used the abovementioned form factor and bcc structure factor. For CCMV-PAMAM samples we used the fcc structure factor. The calculations take into account the form factor of CCMV and position of CCMV within the unit cell whereas the contributions from the other components (avidin or PAMAM-G6 dendrimers) are ignored as their scattering contribution is small compared to CCMV.

6. Supplementary References

1. Kraus, W. & Nolzeb, G. POWDER CELL – a program for the representation and manipulation of crystal structures and calculation of the resulting X-ray powder patterns. *J. Appl. Cryst.* **29,** 301–303 (1996).
2. Förster, S., Apostol, L. & Bras, W. Scatter : software for the analysis of nano- and mesoscale small-angle scattering. *J. Appl. Cryst.* **43,** 639–646 (2010).
3. Förster, S. *et al.* Calculation of scattering-patterns of ordered nano- and mesoscale materials. *Adv. Coll. Int. Sci.* **163,** 53–83 (2011).
4. Kostiainen, M. A. *et al.* Electrostatic assembly of binary nanoparticle superlattices using protein cages. *Nat. Nanotech.* **8,** 52–56 (2013).
5. Josephy, P. D., Eling, T. & Mason, R. P. The horseradish peroxidase-catalyzed oxidation of 3,5,3',5'-tetramethylbenzidine. Free radical and charge-transfer complex intermediates. *J. Biol. Chem.* **257,** 3669–3675 (1982).
6. M. C. Aragonès, The cowpea chlorotic mottle virus as a building block in nanotechnology, PhD thesis, Radboud University Nijmegen, Nijmegen, Netherlands (2010).
7. Speir, J. A., Munshi, S., Wang, G., Baker, T. S. & Johnson, J. E. Structures of the native and swollen forms of cowpea chlorotic mottle virus determined by X-ray crystallography and cryo-electron microscopy. *Structure* **3,** 63–78 (1995).